Biophysics Reviews REVIEW scitation.org/journal/bpr

Interplay of long-chain tetrazine derivatives and biomembrane components at the air–water interface

Cite as: Biophysics Rev. 3, 021303 (2022); doi: 10.1063/5.0083352
Submitted: 24 December 2021 · Accepted: 5 April 2022 ·
Published Online: 28 April 2022

Hiromichi Nakahara,[1] Masayori Hagimori,[2] Takahiro Mukai,[3] and Osamu Shibata[4,a)]

AFFILIATIONS

[1]Department of Industrial Pharmacy, Faculty of Pharmaceutical Sciences, Daiichi University of Pharmacy, 22-1 Tamagawa-cho, Minami-ku Fukuoka 815-8511, Japan
[2]Laboratory of Analytical Chemistry, Faculty of Pharmaceutical Sciences, Mukogawa Women's University, 11-68 Koshien Kyubancho, Nishinomiya 663-8179, Japan
[3]Laboratory of Biophysical Chemistry, Kobe Pharmaceutical University, 4-19-1 Motoyama Kitamachi, Higashinada-ku, Kobe 658-8558, Japan
[4]Department of Biophysical Chemistry, Graduate School of Pharmaceutical Sciences, Nagasaki International University, 2825-7 Huis Ten Bosch, Sasebo, Nagasaki 859-3298, Japan

[a)]**Author to whom correspondence should be addressed**: wosamu@niu.ac.jp. **Tel./Fax:** +81-956-20-5686.
URL: http://www.niu.ac.jp/~pharm1/lab/physchem/indexenglish.html

ABSTRACT

Tetrazine (Tz) is an emerging bioorthogonal ligand that is expected to have applications (e.g., bioimaging) in chemistry and chemical biology. In this review, we highlight the interactions of reduced tetrazine (rTz) derivatives insoluble in aqueous media with biological membrane constituents or their related lipids, such as dipalmitoyl-phosphatidylcholine, dipalmitoyl-phosphatidylethanolamine, dipalmitoyl-phosphatidylglycerol, palmitoyl-sphingomyelin, and cholesterol in the Langmuir monolayer state at the air–water interface. The two-component interaction was thermodynamically elucidated by measuring the surface pressure (π) and molecular area (A) isotherms. The monolayer miscibility between the two components was analyzed using the excess Gibbs energy of mixing and two-dimensional phase diagram. The phase behavior of the binary monolayers was studied using the Brewster angle, fluorescence, and atomic force microscopy. This study discusses the affinities of the rTz moieties for the hydrophilic groups of the lipids used.

TABLE OF CONTENTS

INTRODUCTION

The inverse electron demand Diels–Alder (IEDDA) reaction of electron-poor dienes such as tetrazine (Tz) derivatives and electron-rich dienophiles such as *trans*-cyclooctene derivatives has been used to produce complex natural molecules and pharmaceutical substances[1,2] since its first reporting.[3] The advantage of the IEDDA reactions is that they produce stable adducts in high yields and N_2 as the by-product, and progress in various media, such as water and organic solvents as well as cellular fluid without catalysis.[4] Furthermore, the IEDDA reactions are relatively fast and have rate constants in the range of many orders of magnitude depending on the reactant structure and reaction media.[4–9] Therefore, the IEDDA reaction is a useful strategy for rapid bioconjugation. Indeed, cycloaddition via the IEDDA reaction has a wide range of applications in amine sensing,[10] cellular microscopy,[7] tumor imaging,[6,11,12] hydrogel synthesis for cell encapsulation,[13–15] and metabolic glycoengineering.[16–20] Particularly, *in vivo* molecular imaging is an important technology in drug discovery and development as well as in

the clinic.[21,22] As you can see from these applications, Tz is not a candidate for a new pharmaceutical drug, but rather the accumulation of Tz-containing carriers in tissues via the IEDDA reaction is very characteristic. This property has been applied to fundamental studies on the accumulation of Tz-containing liposomes in cancer tissues and subsequent drug release.[23,24] Hence, it is necessary to understand the movement and distribution of reactants and products of the IEDDA reactions in the living body. Moreover, the interaction between Tz derivatives and cell membranes is very important for the accumulation of Tz-containing liposomes in tissues and organs and is deeply related to the release efficiency of the encapsulated drug.

The basic constituents of biological membranes or biomembranes are mainly lipids and proteins. A lipid molecule is an amphipathic substance with hydrophilic and hydrophobic moieties. Biomembranes are rich in lipids having a glycerol 3-phosphate skeleton or glycerophospholipids, the phosphate groups of which are bonded to the alcohol hydroxyl groups. The non-polar part of the lipids is typically a long-chain fatty acid bound to the polar part of glycerol 3-phosphate. Glycerophospholipids include phosphatidylcholines (PCs), phosphatidylethanolamines (PEs), phosphatidylglycerols (PGs), and phosphatidylserine (PS). Sphingolipids, which are also abundant in cell membranes and nervous system tissues, are based on the sphingosine skeleton and include sphingomyelins (SMs) and cerebrosides. Cholesterol (Ch) is a component of animal cell membranes, although it does not exist in plants and prokaryotes. These lipids form the bilayer structures of cell membranes.[25] The bilayer is composed of two asymmetric leaflets of biomembranes.[26,27] The outer leaflet of the bilayer is enriched in PC, SM, and Ch, whereas the inner leaflet is mainly enriched in PE and PS. PG is a minor component of plasma membrane but exists specifically in pulmonary surfactants.[28–30] Ch plays an important role in controlling membrane fluidity and in the maintenance of SM-rich microdomains or lipid rafts, which are related to membrane signaling and protein trafficking.[31,32]

The methods such as confocal microscopy and dynamic light scattering have been often used for understanding the stability of transport carriers, internalization state of drugs and genes, and their selective accumulation in tissues. However, it is very difficult to elucidate the interaction at the molecular level with these methods. The Langmuir monolayer, which is an insoluble mono-molecular film, can be easily formed at the air–water interface by using the lipids of the biomembrane as constituents. The monolayer technique can evaluate the physical properties in a two-dimensional plane, which is one dimension down from the curved three-dimensional interface seen in cell membranes and liposomes, making it easier to analyze molecular interactions. A characterization of the monolayer generates useful information regarding the interaction among the film-forming materials.[33] The monolayers mimic the leaflets of biological membranes and are adopted as an experimental paradigm to elucidate lateral interaction from the thermodynamic and morphological perspectives.[34–36] The monolayer state at surface pressures of 30–35 mN m^{-1} corresponds to the physical behavior of biomembranes.[37,38] Therefore, researchers in surface chemistry have often employed the Langmuir monolayer to clarify the interfacial behavior of natural lipids and synthesized molecules.[39–41]

In this review, we focused on reduced Tz (rTz) derivatives that comprise a single stearoyl (C18) chain (abbreviated rTz-C18) and two C18 chains (C18-rTz-C18), as shown in Fig. 1. Incorporation of the C18 chains results in the insolubilization of the aqueous medium. In molecular imaging with Tz molecules *in vivo*, the product conjugated to the tumor cell via the IEDDA reaction influences the surrounding biomembranes.[42,43] Thus, the binary interactions between the rTz derivatives and biomembrane constituents, that is, dipalmitoyl-PC (DPPC), dipalmitoyl-PE (DPPE), dipalmitoyl-PG (DPPG), palmitoyl-SM (PSM), and Ch, have been described here. DPPC, DPPG, DPPG,

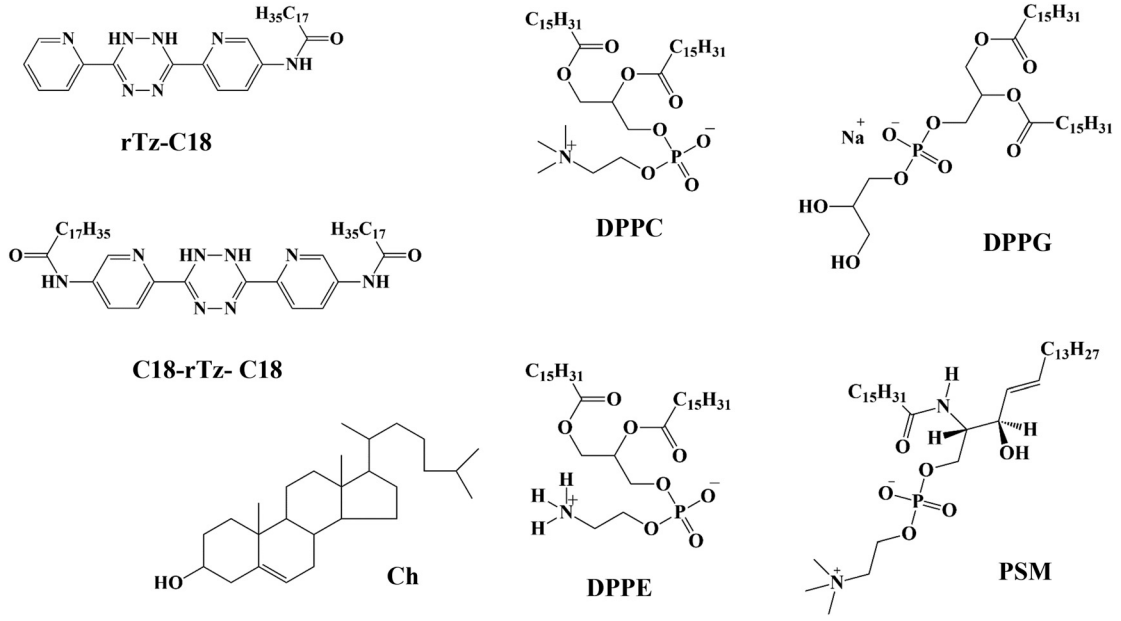

FIG. 1. Chemical structures of rTz-C18, C18-rTz-C18, DPPC, DPPE, DPPG, PSM, and Ch.

and PSM have the same hydrophobic chain. Thus, the difference in their structures is at the level of the hydrophilic groups (Fig. 1), which makes it easy to understand the binary interaction between the rTz moiety and lipid headgroups in the monolayer state.

ISOTHERMAL BEHAVIOR

The surface pressure (π)–molecular area (A) isotherms of the binary monolayers of the (a) DPPC/rTz, (b) DPPE/rTz, (c) DPPG/rTz, (d) PSM/rTz, and (e) Ch/rTz systems are shown in Fig. 2. rTz-C18 (dotted curves in the lower panels) and C18-rTz-C18 (solid curves 5 in the upper panels) form a typical liquid-condensed (LC) monolayer with low compressibility in 0.02 M Tris buffer containing 0.13 M NaCl (pH 7.4) at 298.2 K. The π–A isotherms of rTz-C18 and C18-rTz-C18 reached monolayer collapse, that is, where the monolayer state was converted to the three-dimensional (3D) bulk state on the surface. The collapse pressures (π^c) of the rTz-C18 and C18-rTz-C18 monolayers were 50 and 37 mN m^{-1}, respectively, indicating a more stable monolayer formation of rTz-C18. The extrapolated area of rTz-C18 (0.38 nm^2) is smaller than that of C18-rTz-C18 (0.57 nm^2). These values were larger than the cross-sectional area of one saturated aliphatic chain (~0.20 nm^2/alkyl chain). This suggests that the hydrophilic group of rTz moiety of rTz-C18 and C18-rTz-C18 monolayers is oriented parallel to the surface rather than perpendicular to it in the close-packed state. In particular, the rTz moiety of C18-rTz-C18 is likely to be oriented almost completely parallel to the surface because of the C18 chains at both ends of rTz groups. Based on the extrapolated area (0.57 nm^2), the rTz group (0.38 nm^2) of rTz-C18 is considered to be oriented at a somewhat tilt against the surface. Considering the π^c value, the surface orientation of the rTz headgroup in rTz-C18 can behave more flexibly against the lateral compression of the monolayers. However, the molecular motion of the rTz headgroup of C18-rTz-C18 was limited by its two C18 chains. As for the lipids, the π–A

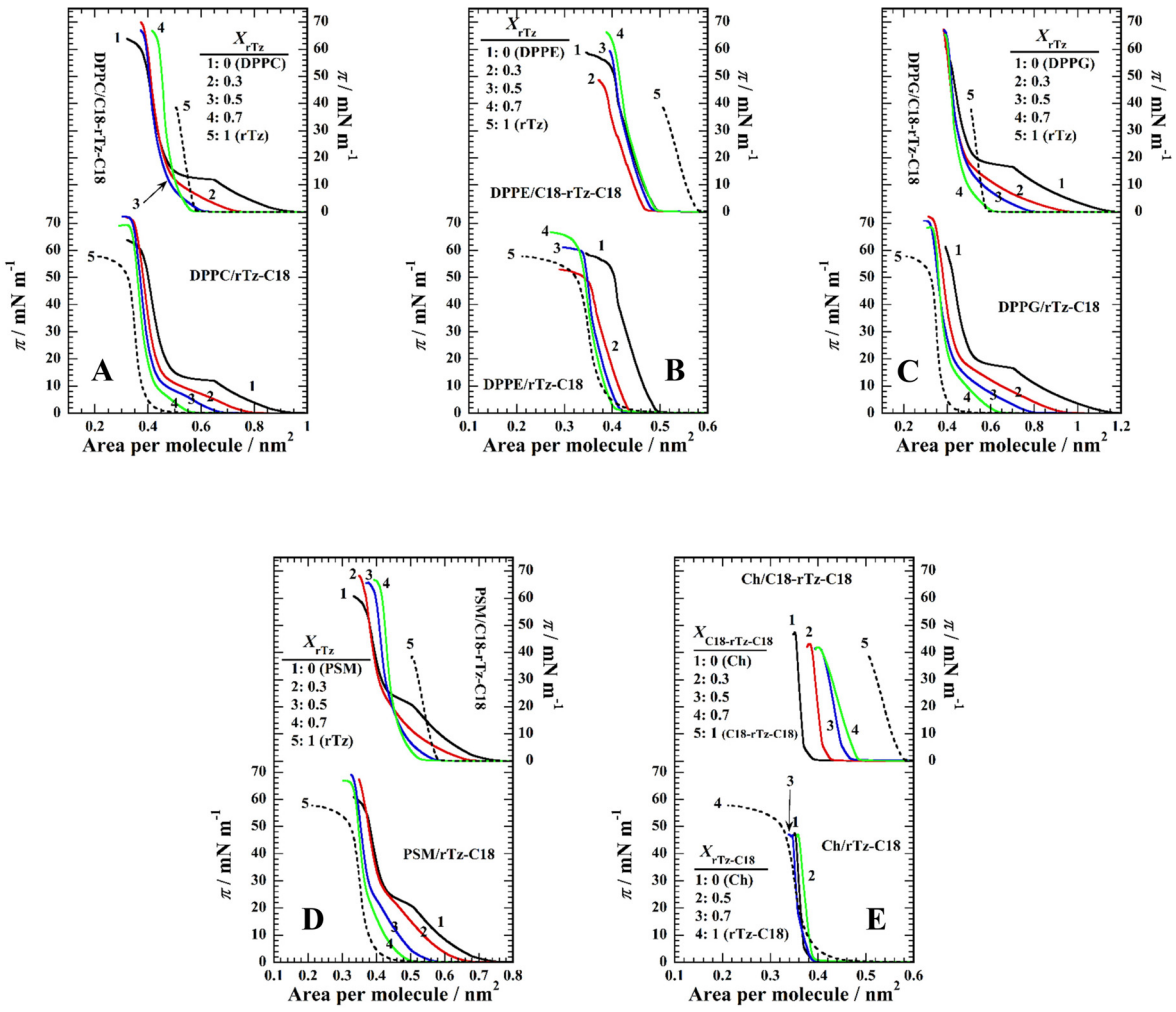

FIG. 2. The π–A isotherms of the two-component (a) DPPC/rTz, (b) DPPE/rTz, (c) DPPG/rTz, (d) PSM/rTz, and (e) Ch/rTz monolayers on 0.02 M Tris buffer solution with 0.13 M NaCl (pH 7.4) at 298.2 K. Reproduced with permission from Nakahara *et al.*, Langmuir **32**, 6591–6599 (2016). Copyright 2016 American Chemical Society. Reproduced with permission from Nakahara *et al.*, Colloids Surf., B **164**, 1–10 (2018). Copyright 2018 Elsevier.

isotherms of DPPC [curve 1 in Fig. 2(a)], DPPG [curve 1 in Fig. 2(c)], and PSM [curve 1 in Fig. 2(d)] exhibit a first-order transition from a liquid-expanded (LE) to an LC phase at a transition pressure, π^{eq} = ∼11 mN m^{-1} (for DPPC), ∼17 mN m^{-1} (for DPPG), and ∼21 mN m^{-1} (for PSM). Thus, these phospholipids formed a more expanded monolayer than rTz-C18 and C18-rTz-C18. In contrast, DPPE [curve 1 in Fig. 2(b)] and Ch [curve 1 in Fig. 2(e)] formed LC monolayers similar to rTz-C18 and C18-rTz-C18.

An interaction can be evaluated from the deviation in the π–A isotherms of single- and two-component systems. The π–A isotherms for the binary lipids/rTz-C18 monolayer (except for the Ch system) regularly shifted within those of the pure components. In particular, the π^{eq} values decrease as the mole fraction of rTz-C18 ($X_{rTz\text{-}C18}$) increases in the DPPC, DPPG, and PSM systems, phenomena that indicate the solidification of the monolayers. The π–A isotherm of the Ch system shows a complicated behavior because the extrapolated areas of Ch and rTz-C18 are approximately the same. The π^{c} value in the DPPC, DPPE, DPPG, and PSM systems changed against $X_{rTz\text{-}C18}$, indicating the miscibility between the two components in the monolayer state. The appearance of the isotherms in the Ch/rTz-C18 binary system strongly reflects that of the Ch isotherm rather than that of rTz-C18. Therefore, Ch contributes significantly to the surface activity and orientation of the two-component monolayer. Unlike other lipids, the hydrophobic moiety of Ch is a bulky steroid backbone. Therefore, the hydrocarbon chains in rTz-C18 and the headgroup interaction between rTz and the OH group (Ch) had little influence on the surface properties. In contrast, the π–A isotherms for the binary monolayers of C18-rTz-C18 and the lipids, such as DPPC, DPPE, DPPG, and PSM, do not line up according to the mole fraction of C18-rTz-C18 ($X_{C18\text{-}rTz\text{-}C18}$) in the upper panels of Figs. 2(a)–2(d). The shift to a small A in the isotherms of the single-component lipids (curve 1) indicates a strong attractive interaction between the two components. Similar to the binary rTz-C18 systems, the addition of C18-rTz-C18 reduced the π^{eq} values and thus induced the solidification of the binary monolayers, except for the DPPE and Ch systems. Furthermore, monolayer miscibility was evidenced by the variation in π^{c} with respect to $X_{C18\text{-}rTz\text{-}C18}$. In contrast, the π–A isotherm of the Ch/C18-rTz-C18 monolayers [upper panel in Fig. 2(e)] was arranged in the order $X_{C18\text{-}rTz\text{-}C18}$. In contrast to the Ch/rTz-C18 system, the two alkyl chains bound to the rTz function without being canceled by the lateral approach of the Ch steroid skeleton.

EXCESS GIBBS ENERGY OF MIXING

The deviation of the experimental π–A isotherms from those estimated under conditions of the ideal mixing of the two components can be calculated from the following equation as the excess Gibbs energy of mixing (ΔG_{mix}^{exc}):[44]

$$\Delta G_{mix}^{exc} = \int_0^{\pi} (A_{12} - X_1 A_1 - X_2 A_2)\mathrm{d}\pi, \quad (1)$$

where A_i and X_i are the molecular area and mole fraction of component i, respectively, and A_{12} is the mean molecular area of the binary monolayer. For identical interactions between the two components, the value of ΔG_{mix}^{exc} is zero; that is, they are ideally mixed in the monolayer or are completely immiscible with each other.[40,45] The variation in ΔG_{mix}^{exc} values against the mole fractions of the rTz derivatives (X_{rTz}) for the binary rTz-C18 and C18-rTz-C18 systems at 35 mN m^{-1} is shown in Fig. 3. A surface pressure of 35 mN m^{-1} is equivalent to that

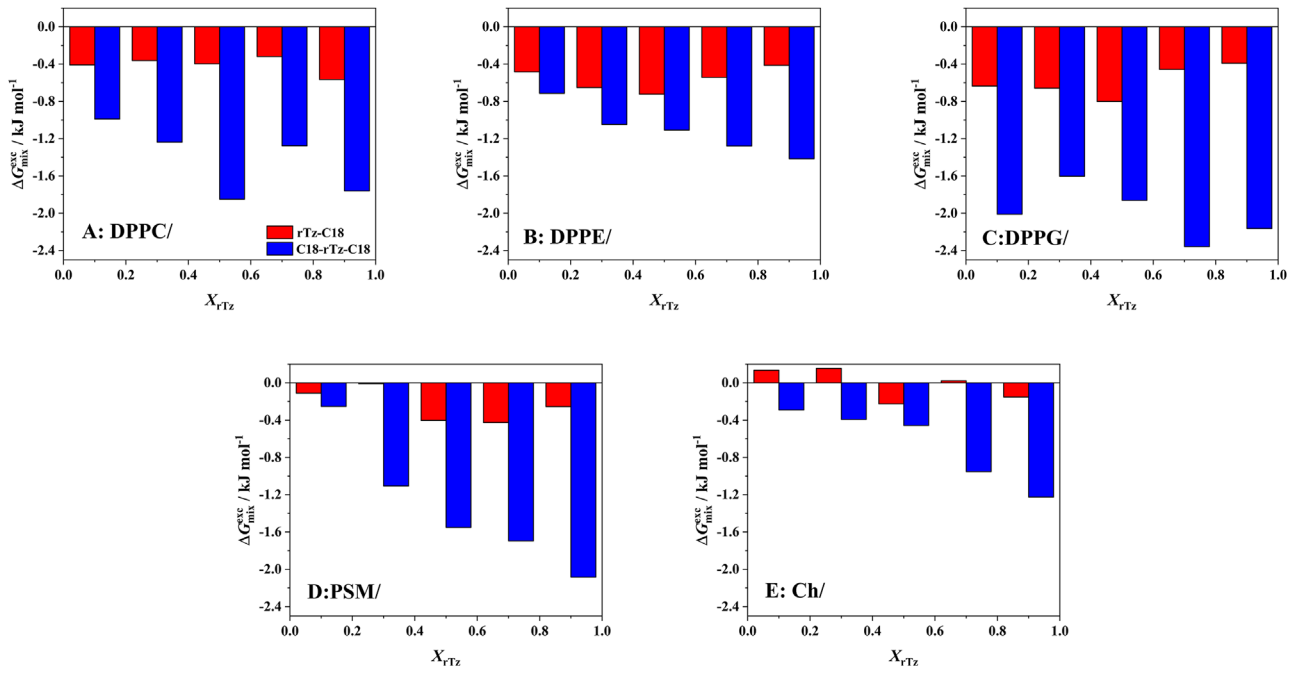

FIG. 3. Excess Gibbs energy of mixing (ΔG_{mix}^{exc}) of the binary (a) DPPC/rTz, (b) DPPE/rTz, (c) DPPG/rTz, (d) PSM/rTz, and (e) Ch/rTz monolayers as a function of mole fraction of rTz ($X_{rTz\text{-}C18}$ or $X_{C18\text{-}rTz\text{-}C18}$) at 35 mN m^{-1} on 0.02 M Tris buffer solution with 0.13 M NaCl (pH 7.4) at 298.2 K. Reproduced with permission from Nakahara *et al.*, Langmuir **32**, 6591–6599 (2016). Copyright 2016 American Chemical Society. Reproduced with permission from Nakahara *et al.*, Colloids Surf., B **164**, 1–10 (2018). Copyright 2018 Elsevier.

of the biological membranes (e.g., 30–35 mN m^{-1}).[37,38] All the systems, except for the Ch/rTz-C18 system [Fig. 3(e)], indicate negative ΔG_{mix}^{exc} values, which means that an attractive interaction exists between the two components. The ΔG_{mix}^{exc} values for DPPC/rTz-C18 [Fig. 3(a)] and PSM/rTz-C18 [Fig. 3(d)] were approximately −0.4 kJ mol^{-1}. The binary monolayers of the DPPE/rTz-C18 [Fig. 3(b)] and DPPG/rTz-C18 [Fig. 3(c)] systems indicate a ΔG_{mix}^{exc} value of nearly −0.6 kJ mol^{-1}. On the contrary, the Ch/rTz-C18 system [Fig. 3(e)] exhibits values between −0.2 and 0.2 kJ mol^{-1}, which suggests the ideal mixing or the immiscibility between Ch and rTz-C18 within a monolayer state. Consequently, the monolayer miscibility and affinity of rTz-C18 at 35 mN m^{-1} for lipids were found to be stronger in the following order: DPPE ≈ DPPG > DPPC ≈ PSM > Ch. Thus, rTz-C18 tends to interact strongly with DPPE and DPPG present in the inner surface of the plasma membrane. Furthermore, there are a few interactions between rTz-C18 and Ch, which are thought to serve as regulators of fluidity in the lipid rafts of plasma membranes.[31,32]

In the binary C18-rTz-C18 system, the ΔG_{mix}^{exc} value was entirely negative, irrespective of X_{rTz}. Furthermore, the absolute ΔG_{mix}^{exc} value was more than twice that of the corresponding rTz-C18 system. This suggested a stronger interplay between the lipids and C18-rTz-C18. Considering the difference in the chemical structures of the rTz derivatives, it is implied that the rTz moiety in C18-rTz-C18 is immobilized at the air–water interface by the two hydrocarbon chains (C18), and it is easier to interact with the hydrophilic group of the lipids. The absolute ΔG_{mix}^{exc} values for the DPPC/C18-rTz-C18 [Fig. 3(a)], DPPG/C18-rTz-C18 [Fig. 3(c)], and PSM/C18-rTz-C18 [Fig. 3(d)] systems were larger than those for the DPPE/C18-rTz-C18 [Fig. 3(b)] and Ch/C18-rTz-C18 [Fig. 3(e)] systems. That is, C18-rTz-C18 interacted more favorably with less rigid monolayers. In addition, it can be said that C18-rTz-C18 interacts more strongly with the lipids in the following order: DPPG > DPPC ≈ PSM > DPPE > Ch. Compared to rTz-C18, the affinity of the rTz moiety in C18-rTz-C18 for DPPE headgroups was considerably inferior. The degree of freedom of the rTz molecular motion at the surface is the key factor for the specific interaction between the PE headgroup and rTz moiety. Moreover, C18-rTz-C18 interacted strongly with the lipids on the outer surface of the lipid bilayers. Contrastingly, Ch tends to interact more attractively with C18-rTz-C18 than rTz-C18, which suggests that the immobilization of the rTz moieties at the air–water interface makes it easier for the rTz moieties to produce the π–π interaction with the Ch steroid backbone.

TWO-DIMENSIONAL (2D) PHASE DIAGRAMS

The 2D phase diagrams at 30 ≤ π ≤ 70 mM m^{-1} for the binary systems (Fig. 4) were constructed by plotting the experimental π^c values against X_{rTz}. In the region below 30 mN m^{-1}, the binary DPPC, DPPG, and PSM systems exhibit a phase transition from the LE to LC states on their π–*A* isotherms (Fig. 2). The π^{eq} value of the binary systems decreases sharply with respect to X_{rTz}, which suggests the solidifying effect of the rTz derivatives on the DPPC, DPPG, and PSM monolayers. The rate of π^{eq} change ($\partial\pi^{eq}/\partial X_{rTz}$) and the critical mole fraction $X^c_{rTz-C18}$, above which the monolayer is in the LC phase at

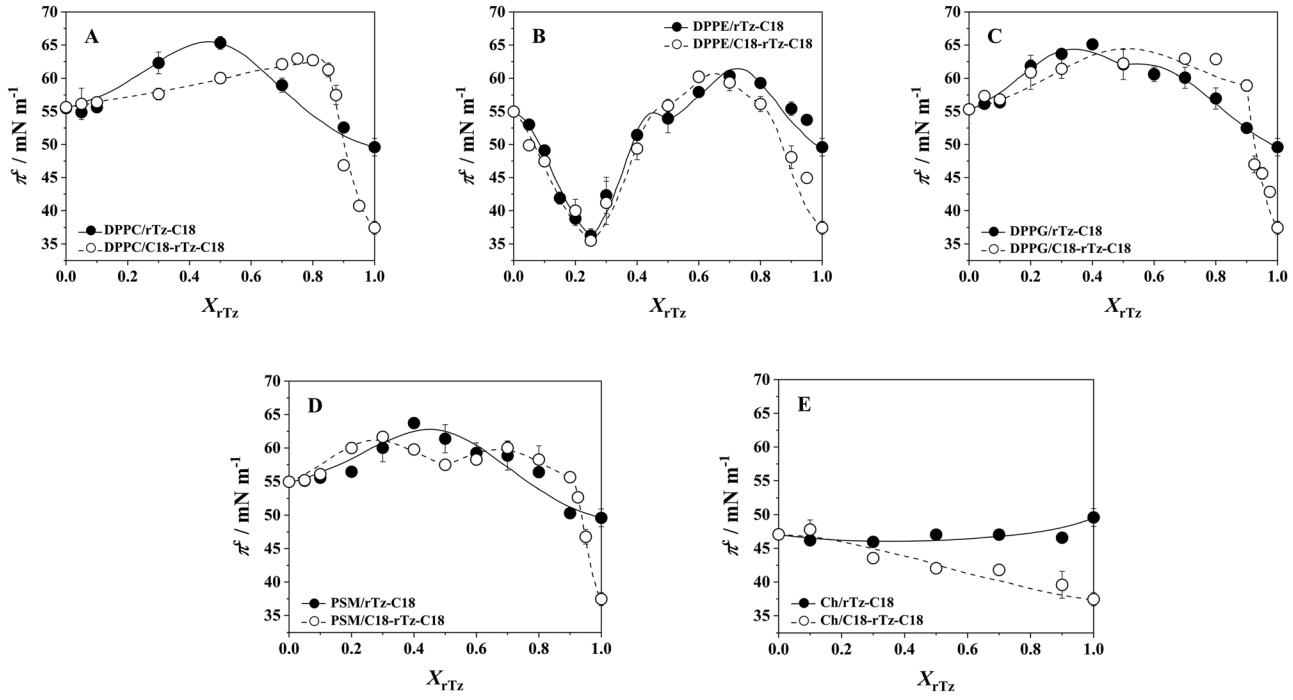

FIG. 4. Two-dimensional phase diagrams based on the variation of the collapse pressure (π^c) on 0.02 M Tris buffer solution with 0.13 M NaCl (pH 7.4) at 298.2 K as a function of rTz ($X_{rTz\text{-}C18}$ or $X_{C18\text{-}rTz\text{-}C18}$). The curved lines were obtained by curve fitting of experimental π^c values to Eq. (2): (a) DPPC/rTz, (b) DPPE/rTz, (c) DPPG/rTz, (d) PSM/rTz, and (e) Ch/rTz. Reproduced with permission from Nakahara *et al.*, Langmuir 32, 6591–6599 (2016). Copyright 2016 American Chemical Society. Reproduced with permission from Nakahara *et al.*, Colloids Surf., B **164**, 1–10 (2018). Copyright 2018 Elsevier.

finite surface pressures, have been discussed in previous studies.[46,47] The experimental π^c values for the binary DPPC, DPPE, DPPG, and PSM systems [Figs. 4(a)–4(d)] change considerably with X_{rTz}. This result provides evidence of the two-component miscibility in the monolayer state. The DPPE/rTz-C18 and DPPE/C18-rTz-C18 systems exhibited complex π^c variations. The π^c profile has a minimum value of ~36 mN m^{-1} at $X_{rTz} = 0.25$, which is smaller than the π^c values of the pure DPPE, rTz-C18, and C18-rTz-C18 monolayers. The decrease in the π^c value at $X_{rTz} = 0.25$ implies an attenuation of the stability of DPPE monolayers against lateral pressures. This means that when rTz approaches the biomembrane constituents from the inside, the attractive interaction between the hydrophilic group of DPPE and rTz can lead to a membrane collapse. The coexistence phase boundary between the monolayer phase (2D) and bulk phase (3D) of the molecules spread on the surface can be theoretically simulated by using the Joos equation[48,49] and assuming a regular surface mixture

$$1 = X_1 \exp\{(\pi^c - \pi_1^c)A_1/kT\}\exp(\xi \cdot X_2^2) + X_2 \exp\{(\pi^c - \pi_2^c)A_2/kT\}\exp(\xi \cdot X_1^2), \quad (2)$$

where X_1 and X_2 represent the mole fractions of components 1 and 2, respectively, in the two-component monolayer; π_1^c and π_2^c are the collapse pressures of components 1 and 2, respectively; A_1 and A_2 are the molecular areas of components 1 and 2 at π_1^c and π_2^c, respectively; ξ is the interaction parameter; and kT is the product of the Boltzmann constant and the absolute temperature. Solid (rTz-C18 systems) and broken (C18-rTz-C18 systems) curves were obtained by adjusting ξ in Eq. (2) to obtain the best fit for the experimentally determined π^c values. Accordingly, the interaction energy ($\Delta\varepsilon$) is expressed as follows:

$$\Delta\varepsilon = \xi RT/z, \quad (3)$$

where z is the number of nearest neighbors per molecule (equal to six in this case) in a closely packed monolayer. The expression for the interaction energy can be rewritten as $\Delta\varepsilon = \varepsilon_{12} - (\varepsilon_{11} + \varepsilon_{22})/2$,[48] where ε_{12} denotes the potential interaction energy between components 1 and 2. The regions above and below the curves represent bulk and monolayer phases, respectively. The ξ and $\Delta\varepsilon$ values for the binary systems are summarized in Table I. The whole $\Delta\varepsilon$ values are smaller than the mean thermal energy ($2RT = \sim 5.0$ kJ mol^{-1} at 298.2 K), which reveals that the molecular interaction related to the binary miscibility is based on the non-bonding intermolecular forces instead of a functional chemical bond, such as a covalent bond. Heterogeneous interactions (e.g., DPPC vs rTz-C18, not DPPC vs DPPC) predominated in all the systems (except the Ch systems) because of the negative ξ and $\Delta\varepsilon$ values. This is also supported by the negative ΔG_{mix}^{exc} values (Fig. 3). Among them, the binary DPPC and PSM systems showed stronger heterogeneous interactions, regardless of the rTz species. The DPPE systems showed a complicated profile of ξ and $\Delta\varepsilon$ values with X_{rTz}; however, the values themselves were almost the same as those of the DPPG systems. However, the Ch/rTz systems indicate a completely different aspect from these systems. In the Ch/rTz-C18 system, homogeneous interactions predominate over heterogeneous interactions because of the positive ξ and $\Delta\varepsilon$ values. However, the ξ and $\Delta\varepsilon$ values of the binary Ch/C18-rTz-C18 system are negative, and thus, the Ch–C18-rTz-C18 interaction occurs more favorably. This difference in the ξ and $\Delta\varepsilon$ values is attributed to the depression of the rTz molecular motion at the surface induced in response to the incorporation of two C18 chains. Nevertheless, the small ξ and $\Delta\varepsilon$ values support nearly ideal mixing between Ch and rTz-C18 as well as between Ch and C18-rTz-C18.

IN SITU MORPHOLOGICAL OBSERVATIONS

The morphological images captured by fluorescence microscopy (FM) provide information regarding the distribution of different monolayer phases and the interaction between them. Figure 5 shows typical FM images of the binary DPPC/rTz, DPPG/rTz, and PSM/rTz monolayers containing 1 mol. % 1-palmitoyl-2-[6-[(7-nitro-2-1,3-benzoxadiazol-4-yl)amino]hexanoyl]-*sn*-glycero-3-phosphocholine (NBD-PC) as a fluorescent probe *in situ* at the air–water interface. Owing to the limited magnification and resolution, the FM images

TABLE I. The interaction parameter (ξ) and the interaction energy ($\Delta\varepsilon$) of the binary DPPC/rTz, DPPE/rTz, DPPG/rTz, PSM/rTz, and Ch/rTz monolayers.

		rTz-C18			C18-rTz-C18			
DPPC	X	$0 \le X \le 1$			$0 \le X \le 0.8$		$0.8 \le X \le 1$	
	ξ	−4.40			−0.16		−3.98	
	$\Delta\varepsilon$ (kJ/mol)	−1.82			−0.07		−1.64	
DPPE	X	$0 \le X \le 0.25$	$0.25 \le X \le 0.5$	$0.5 \le X \le 1$	$0 \le X \le 0.25$	$0.25 \le X \le 0.5$	$0.5 \le X \le 0.8$	$0.8 \le X \le 1$
	ξ	−1.32	−2.53	−3.13	−1.23	−2.19	−1.92	−2.00
	$\Delta\varepsilon$ (kJ/mol)	−0.55	−1.05	−1.29	−0.51	−0.90	−0.79	−0.83
DPPG	X	$0 \le X \le 0.5$		$0.5 \le X \le 1$	$0 \le X \le 0.9$		$0.9 \le X \le 1$	
	ξ	−1.96		−1.20	−2.82		−1.08	
	$\Delta\varepsilon$ (kJ/mol)	−0.81		−0.50	−1.17		−0.45	
PSM	X	$0 \le X \le 1$			$0 \le X \le 0.5$	$0.5 \le X \le 0.9$	$0.9 \le X \le 1$	
	ξ	−3.50			−1.82	−1.25	−2.19	
	$\Delta\varepsilon$ (kJ/mol)	−1.45			−0.75	−0.52	−0.90	
Ch	X	$0 \le X \le 1$				$0 \le X \le 1$		
	ξ	0.66				−1.05		
	$\Delta\varepsilon$ (kJ/mol)	0.27				−0.43		

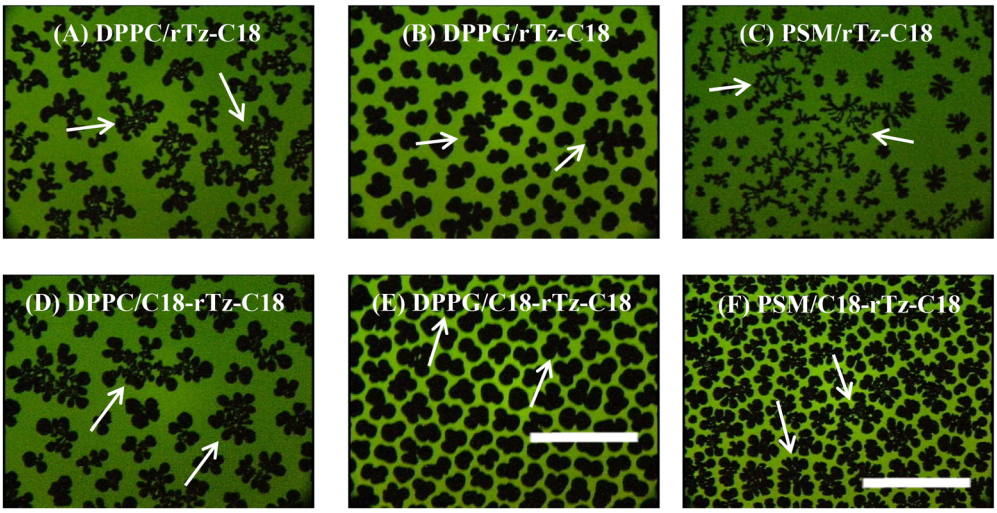

FIG. 5. FM images of the binary DPPC/rTz, DPPG/rTz, and PSM/rTz monolayers for $X_{rTz\text{-}C18} = 0.3$ on 0.02 M Tris buffer solution with 0.13 M NaCl (pH 7.4) at 298.2 K. The monolayers contained 1 mol. % Fluorescent probe (NBD-PC). The scale bar in the lower right represents 100 μm: (a) 10 mN m^{-1}, (b) 15 mN m^{-1}, (c) 15 mN m^{-1}, (d) 5 mN m^{-1}, (e) 17 mN m^{-1}, and (f) 20 mN m^{-1}. Reproduced with permission from Nakahara *et al.*, Langmuir **32**, 6591–6599 (2016). Copyright 2016 American Chemical Society. Reproduced with permission from Nakahara *et al.*, Colloids Surf., B **164**, 1–10 (2018). Copyright 2018 Elsevier.

for the DPPE/rTz and Ch/rTz systems were kept homogeneously dark, regardless of X_{rTz} and π. In the FM observation, a small amount of fluorescent probe (approximately 1 mol. %) was doped into the monolayer. The fluorescent probe was selectively dissolved in the LE phases of the monolayers because of its bulky structure. Thus, the LE phase of the monolayer was imaged as a bright contrast in the FM images. Bright and dark domains coexisted in the FM image of the binary DPPC/rTz-C18 monolayer [Fig. 5(a)]. The dark domain had a complex shape with branched arms. The domain shape is commonly controlled by the balance of the line tension at the boundary between the LE and LC domains and a long-range dipole–dipole interaction between the LC domains.[50–56] The FM image revealed the presence of two kinds of LC domains, that is, a DPPC-rich domain (20–30 μm in diameter) and a domain formed by the miscible monolayer of DPPC and rTz-C18 ($\sim$50 μm in diameter, indicated by white arrows).[47] The domains made of the miscible monolayer transform into a noncircular form, which signifies the enhancement of the dipole–dipole repulsive interaction among the LC domains by the rTz-C18 incorporation. The formation of two different LC domains is not attributed to the interaction with the probe because the same morphological image is observed in the *in situ* Brewster angle microscopy (BAM) images.[47] BAM demonstrated that the LC domains derived from DPPC–rTz-C18 mixed monolayers are more rigid and have a higher density than those of the DPPC monolayers. Similar morphological phenomena were observed for the binary DPPC/C18-rTz-C18 system [Fig. 5(d)]. Thus, the interaction between the rTz moieties and DPPC headgroup resulted in the formation of two different LC domains. Furthermore, FM of the DPPG/rTz [Figs. 5(b) and 5(e)] and PSM/rTz [Figs. 5(c) and 5(f)] monolayers revealed the presence of two types of LC phases. This indicates that the two components are not completely miscible within a monolayer, but instead are partially miscible.

ATOMIC FORCE MICROSCOPY (AFM) OBSERVATIONS

AFM cannot be used to observe a monolayer *in situ* at the air–water interface, but it can be used to observe a monolayer transferred to a solid substrate such as mica at a higher magnification and resolution. The AFM images of the Langmuir–Blodgett (LB) films transferred

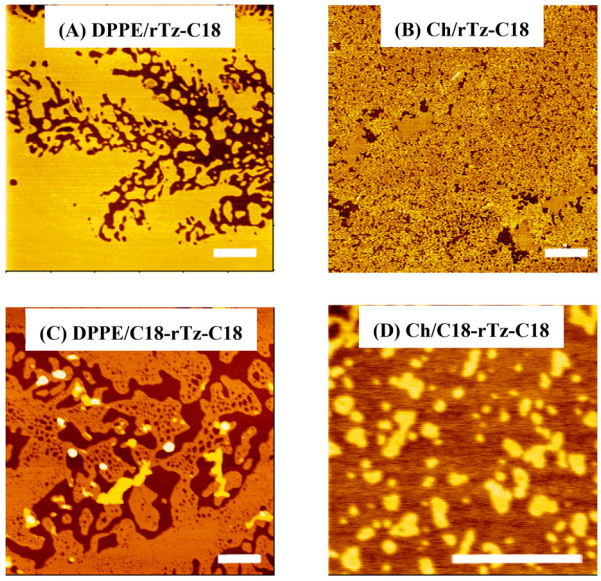

FIG. 6. Typical AFM topographic images of the binary DPPE/rTz and Ch/rTz monolayers at 35 mN m^{-1}. The scale bar in the lower right represents 500 μm: (a) $X_{rTz\text{-}C18} = 0.5$, (b) $X_{rTz\text{-}C18} = 0.5$, (c) $X_{C18\text{-}rTz\text{-}C18} = 0.7$, and (d) $X_{C18\text{-}rTz\text{-}C18} = 0.7$. Reproduced with permission from Nakahara *et al.*, Langmuir **32**, 6591–6599 (2016) Copyright (2016) American Chemical Society. and Colloids Surf., B 164, 1–10 (2018). Copyright 2018 Elsevier.

from the binary DPPE/rTz and Ch/rTz monolayers at 35 mN m^{-1} are shown in Fig. 6. Dark (DPPE) and bright (rTz-C18) domains were observed in the images of the DPPE/rTz-C18 LB films [Fig. 6(a)]. The incorporation of rTz-C18 had a highly dispersing effect on the DPPE monolayers. Furthermore, rTz-C18 was completely miscible in DPPE over the entire $X_{rTz\text{-}C18}$.[47] The dispersion effect associated with the addition of C18-rTz-C18 on the DPPE monolayers was also observed in the DPPE/C18-rTz-C18 system [Fig. 6(c)]. The headgroups of DPPC and DPPE are zwitterions at neutral pH. The structural difference between DPPC and DPPE is only the headgroup, that is, a choline group (DPPC) and an amino group (DPPE). However, the additional effect of the rTz derivatives on the DPPC and DPPE monolayers was completely different. Therefore, it was demonstrated that the amino group interaction sites in the lipid structures are a key factor underlying the dispersing effect of the rTz group on biomembranes. This dispersing effect contributes to monolayer instability or π^c reduction in the DPPE/rTz systems [Fig. 4(b)].

In the Ch/rTz-C18 system at $X_{rTz\text{-}C18} = 0.5$ [Fig. 6(b)], AFM reveals a highly dispersed pattern; the dark and bright domains are assigned to Ch and rTz-C18 monolayers, respectively.[47] Thus, considering the thermodynamic results mentioned above, it can be said that Ch and rTz are closer to the ideal mixture in the monolayer state rather than the immiscible mixture. AFM of the binary Ch/C18-rTz-C18 system [Fig. 6(d)] revealed the coexistence of dark (mainly Ch) and bright (C18-rTz-C18) domains. The height difference between the two domains was approximately 1.4 nm, which is much lower than the molecular length of Ch and C18-rTz-C18. However, this value was somewhat large because of the difference in the molecular lengths of the two compounds. This can be explained by the fact that the π–π interaction between the steroid backbone (Ch) and the rTz moiety (C18-rTz-C18) slightly lifts the rTz moiety of C18-rTz-C18 from the air–water interface to the air phase. This morphological behavior is also observed in the AFM image for Ch/rTz-C18 at $X_{rTz\text{-}C18} = 0.7$.[47] Furthermore, the bright domain shape is neither uniform nor circular in Fig. 6(d). This indicates the variation in the line tension at the phase boundary, which supports binary miscibility in the monolayer state.

CONCLUSION

rTz derivatives, such as rTz-C18 and C18-rTz-C18, formed a stable Langmuir monolayer characterized by the presence of LC phases in the present experimental conditions. The binary interactions between the monolayers of the rTz derivatives and biomembrane constituents of DPPC, DPPE, DPPG, PSM, and Ch are attractive and miscible from thermodynamic and morphological perspectives. Among them, the interaction with Ch is relatively weak; in particular, the Ch/rTz-C18 system exhibits ideal mixing. Based on the thermodynamic evaluations, the two-component miscibility of rTz-C18 and C18-rTz-C18 with the lipids increased in the following order: DPPE > DPPG > DPPC ≈ PSM > Ch and DPPG > DPPC ≈ PSM > DPPE > Ch. The rTz headgroup exhibits a large difference in affinity with the DPPE headgroup, depending on whether it has one or two C18 chains. The C18 chain controls the molecular motion of the rTz moieties at the air–water interface and has a significant influence on the interaction with other molecules.

BAM and FM revealed the coexistence of two types of LC domains made of phospholipids and phospholipid-rTz mixtures for the DPPC/rTz, DPPG/rTz, and PSM/rTz systems. This coexistence indicates a quantitatively limited ratio of interaction between the two components. In contrast, AFM suggests that the interaction between the Ch and the rTz derivatives is quite different from the interaction of the other two-component systems and is based on the π–π interaction between the steroid backbone (Ch) and rTz moiety.

rTz and the amino group exhibit a very characteristic interaction. DPPC and DPPE have similar structures; however, they interact differently with rTz. DPPC improves monolayer stability (or durability of the monolayer against lateral pressure) by adding rTz. However, the addition of DPPE results in a decrease in monolayer stability. The decrease in the collapse pressure (∼35 mN m^{-1}) is comparable to the surface pressure of the biomembrane, suggesting that the interaction of rTz with the amino group of DPPE may cause the biological membrane to collapse from the inside of cells.

ACKNOWLEDGMENTS

This work was supported by a Grant-in-Aid for Scientific Research No. 19K07036 from the Japan Society for the Promotion of Science (JSPS).

AUTHOR DECLARATIONS

Conflict of Interest

The authors have no conflicts to disclose.

DATA AVAILABILITY

Data sharing is not applicable to this article as no new data were created or analyzed in this study.

REFERENCES

[1]K. C. Nicolaou, S. A. Snyder, T. Montagnon, and G. Vassilikogiannakis, Angew. Chem., Int. Ed. **41**(10), 1668–1698 (2002).
[2]J.-A. Funel and S. Abele, Angew. Chem., Int. Ed. **52**(14), 3822–3863 (2013).
[3]R. A. Carboni and R. V. Lindsey, J. Am. Chem. Soc. **81**(16), 4342–4346 (1959).
[4]M. L. Blackman, M. Royzen, and J. M. Fox, J. Am. Chem. Soc. **130**(41), 13518–13519 (2008).
[5]N. K. Devaraj, R. Weissleder, and S. A. Hilderbrand, Bioconj. Chem. **19**(12), 2297–2299 (2008).
[6]R. Rossin, P. Renart Verkerk, S. M. van den Bosch, R. C. M. Vulders, I. Verel, J. Lub, and M. S. Robillard, Angew. Chem., Int. Ed. **122**(19), 3447–3450 (2010).
[7]N. K. Devaraj and R. Weissleder, Acc. Chem. Res. **44**(9), 816–827 (2011).
[8]K. Lang, L. Davis, S. Wallace, M. Mahesh, D. J. Cox, M. L. Blackman, J. M. Fox, and J. W. Chin, J. Am. Chem. Soc. **134**(25), 10317–10320 (2012).
[9]R. Rossin, S. M. van den Bosch, W. ten Hoeve, M. Carvelli, R. M. Versteegen, J. Lub, and M. S. Robillard, Bioconj. Chem. **24**(7), 1210–1217 (2013).
[10]J. Malinge, C. Allain, L. Galmiche, F. Miomandre, and P. Audebert, Chem. Mater. **23**(20), 4599–4605 (2011).
[11]Z. Ni, L. Zhou, X. Li, J. Zhang, and S. Dong, PLoS One **10**(11), e0141918 (2015).
[12]D. A. Roberts, B. S. Pilgrim, J. D. Cooper, T. K. Ronson, S. Zarra, and J. R. Nitschke, J. Am. Chem. Soc. **137**(32), 10068–10071 (2015).
[13]D. F. Martin, M. G. Maguire, G.-s. Ying, J. E. Grunwald, S. L. Fine, and G. J. Jaffe, N. Engl. J. Med. **364**(20), 1897–1908 (2011).
[14]S. Koutsopoulos and S. Zhang, J. Controlled Release **160**(3), 451–458 (2012).
[15]C. E. Ziegler, M. Graf, M. Nagaoka, H. Lehr, and A. M. Goepferich, Biomacromolecules **22**(8), 3223–3236 (2021).
[16]P. R. Wratil, R. Horstkorte, and W. Reutter, Angew. Chem., Int. Ed. **55**(33), 9482–9512 (2016).
[17]T. J. Sminia, H. Zuilhof, and T. Wennekes, Carbohydrate Res. **435**, 121–141 (2016).
[18]L. K. Mahal, K. J. Yarema, and C. R. Bertozzi, Science **276**(5315), 1125–1128 (1997).

[19]K. K. Palaniappan and C. R. Bertozzi, Chem. Rev. **116**(23), 14277–14306 (2016).
[20]H. Kayser, R. Zeitler, C. Kannicht, D. Grunow, R. Nuck, and W. Reutter, J. Biol. Chem. **267**(24), 16934–16938 (1992).
[21]P. M. Matthews, E. A. Rabiner, J. Passchier, and R. N. Gunn, Br. J. Clin. Pharmacol. **73**(2), 175–186 (2011).
[22]R. J. Hargreaves, Clin. Pharmacol. Ther. **83**(2), 349–353 (2008).
[23]K. Kannaka, K. Sano, M. Hagimori, T. Yamasaki, M. Munekane, and T. Mukai, Bioorg. Med. Chem. **27**(16), 3613–3618 (2019).
[24]K. Kannaka, K. Sano, H. Nakahara, M. Munekane, M. Hagimori, T. Yamasaki, and T. Mukai, Langmuir **36**(36), 10750–10755 (2020).
[25]S. J. Singer and G. L. Nicolson, Science **175**(4023), 720–731 (1972).
[26]M. S. Bretscher, Nature **236**, 11–12 (1972).
[27]D. L. Daleke, J. Lipid Res. **44**(2), 233–242 (2003).
[28]R. Veldhuizen, K. Nag, S. Orgeig, and F. Possmayer, Biochim. Biophys. Acta **1408**(2–3), 90–108 (1998).
[29]P. Krüger, J. E. Baatz, R. A. Dluhy, and M. Lösche, Biophys. Chem. **99**(3), 209–228 (2002).
[30]S.-H. Yu and F. Possmayer, J. Lipid Res. **44**(3), 621–629 (2003).
[31]K. Simons and E. Ikonen, Nature **387**(6633), 569–572 (1997).
[32]K. Simons and D. Toomre, Nat. Rev. Mol. Cell Biol. **1**, 31–39 (2000).
[33]G. L. Gaines, Jr., *Insoluble Monolayers at Liquid-Gas Interfaces* (Interscience Publishers, New York, 1966).
[34]V. von Tscharner and H. M. McConnell, Biophys. J. **36**(2), 421–427 (1981).
[35]R. Peters and K. Beck, Proc. Natl. Acad. Sci. U. S. A. **80**(23), 7183–7187 (1983).
[36]V. von Tscharner and H. M. McConnell, Biophys. J. **36**(2), 409–419 (1981).
[37]D. Marsh, Biochim. Biophys. Acta, Rev. Biomembr. **1286**(3), 183–223 (1996).
[38]M. J. Conrad and S. J. Singer, Proc. Natl. Acad. Sci. U. S. A. **76**(10), 5202–5206 (1979).
[39]J. G. Petrov, T. Pfohl, and H. Möhwald, J. Phys. Chem. B **103**, 3417–3424 (1999).
[40]D. O. Shah and J. H. Schulman, J. Lipid Res. **8**(3), 215–226 (1967).
[41]T. H. Chou and C. H. Chang, Colloids Surf., B **17**(2), 71–79 (2000).
[42]H. Li, J. Conde, A. Guerreiro, and G. J. L. Bernardes, Angew. Chem., Int. Ed. **59**(37), 16023–16032 (2020).
[43]X. Ji, Z. Pan, B. Yu, L. K. De La Cruz, Y. Zheng, B. Ke, and B. Wang, Chem. Soc. Rev. **48**(4), 1077–1094 (2019).
[44]F. C. Goodrich, in Proceeding of 2nd International Congress on Surface Activity; edited by J. H. Schulman (Butterworth & Co., London, 1957) p 85.
[45]J. Marsden and J. H. Schulman, Trans. Faraday Soc. **34**, 748–758 (1938).
[46]H. Nakahara, M. Hagimori, T. Mukai, and O. Shibata, Colloids Surf., B **164**, 1–10 (2018).
[47]H. Nakahara, M. Hagimori, T. Mukai, and O. Shibata, Langmuir **32**(26), 6591–6599 (2016).
[48]P. Joos and R. A. Demel, Biochim. Biophys. Acta, Biomembr. **183**(3), 447–457 (1969).
[49]M. Savva and S. Acheampong, J. Phys. Chem. B **113**(29), 9811–9820 (2009).
[50]H. M. McConnell, Annu. Rev. Phys. Chem. **42**, 171–195 (1991).
[51]D. J. Keller, H. M. McConnell, and V. T. Moy, J. Phys. Chem. **90**, 2311–2315 (1986).
[52]D. J. Keller, J. P. Korb, and H. M. McConnell, J. Phys. Chem. **91**, 6417–6422 (1987).
[53]V. T. Moy, D. J. Keller, and H. M. McConnell, J. Phys. Chem. **92**, 5233–5238 (1988).
[54]H. M. McConnell, J. Phys. Chem. **94**, 4728–4731 (1990).
[55]D. J. Benvegnu and H. M. McConnell, J. Phys. Chem. **96**, 6820–6824 (1992).
[56]D. J. Benvegnu and H. M. McConnell, J. Phys. Chem. **97**, 6686–6691 (1993).